Journal of Innovative Optical Health Sciences
Vol. 13, No. 3 (2020) 2050011 (11 pages)

DOI: 10.1142/S179354582050011X

Interaction between Bax and Bcl-XL proteins confirmed by partial acceptor photobleaching-based FRET imaging

Fangfang Yang*, Mengyan Du*, Xiaoping Wang†,‡,¶ and Tongsheng Chen*,§,¶
*MOE Key Laboratory of Laser Life Science and College of Biophotonics
South China Normal University
Guangzhou 510631, P. R. China
†Department of Pain Management
the First Affiliated Hospital of Jinan University
Guangzhou 510630, P. R. China
‡txp2938@jnu.edu.cn
§chentsh@scnu.edu.cn; chentsh126@126.com

Received 28 September 2019
Accepted 19 January 2020
Published 26 February 2020

Exact interaction mechanism between Bax and Bcl-XL, two key Bcl-2 family proteins, is an interesting and controversial issue. Partial acceptor photobleaching-based quantitative fluorescence resonance energy transfer (FRET) measurement, PbFRET, is a widely used FRET quantification method in living cells. In this report, we implemented pixel-to-pixel PbFRET imaging on a wide-field microscope to map the FRET efficiency (E) images of single living HepG2 cells co-expressing CFP-Bax and YFP-Bcl-XL. The E value between CFP-Bax and YFP-Bcl-XL was 4.59% in cytosol and 11.31% on mitochondria, conclusively indicating the direct interaction of the two proteins, and the interaction of the two proteins was strong on mitochondria and modest in cytosol.

Keywords: Bax; Bcl-XL; protein–protein interaction; FRET imaging; living cells.

1. Introduction

Bax and Bcl-XL proteins, two members of the Bcl-2 family proteins, play a key role in the 'mitochondrial' or 'intrinsic' apoptosis pathway.[1,2] It is generally considered that proapoptotic protein Bax resides in the cytoplasm of healthy cells and translocates to the mitochondrial outer membrane (MOM) and oligomerizes upon apoptosis induction,[3–5] while anti-apoptotic protein Bcl-XL presenting in both cytoplasm and mitochondria in untreated cells is generally considered to inhibit Bax activation.[6–9] However, the exact interaction

¶Corresponding authors.

mechanism between the two proteins is still an interesting issue in the last two decades.

Bcl-XL was considered to directly interact with Bax to inhibit Bax activation 20 years ago.[10,11] However, this notion was difficult to reconcile with the immunoprecipitation experimental evidence that Bcl-XL did not interact with Bax in cytosol.[12,13] Subsequently, Bcl-XL was proposed to compete with Bax for membrane and tBid binding in liposomes or isolated mitochondria to inhibit Bax binding to mitochondria,[14,15] which was contradicted with the observations that Bcl-XL was able to stimulate Bax mitochondrial translocation in Hela cells[16] and Bcl-XL stabilized mitochondrial-associated Bax to reduce the dissociation rate of mitochondrial Bax.[17] Moreover, Schellenberg *et al.* proposed a novel notion that Bax constitutively targeted to mitochondria was constantly translocated back to the cytosol in nonapoptotic cells, and Bax dissociation from the mitochondria occurred independently of Bcl-2 survival proteins and direct-activator BH3 proteins.[17] The latest study identified that Bcl-XL stimulated Bax relocation to mitochondria and primed mitochondria to permeabilization and cytochrome c release.[18] In contrast to this notion, fluorescence loss in photobleaching (FLIP) and fluorescence recovery after photobleaching (FRAP) analysis in single living cells demonstrated that Bcl-XL interacted with Bax on mitochondria to enhance Bax relocalization from mitochondria to the cytosol in nonapoptotic cells.[3,19]

Fluorescence resonance energy transfer (FRET) is a powerful tool for quantitative analysis of protein–protein interaction, protease and kinase activities in living cells.[6,20,21] Genetically encoded fluorescent proteins (FPs)-based biosensors make FRET technology capable of resolving dynamic signaling events inside living cells in situ and without influence normal physiological activities.[22,23] Complete acceptor photobleaching is the most straightforward method to detect FRET,[24,25] which does not require external references and system calibration.[26] However, complete photobleaching generally takes several minutes, which may induce serious photodamage to living cells.[27] Partial acceptor photobleaching-based quantitative FRET measurement (PbFRET) developed by Elder *et al.*[28] and Wang *et al.*[29] only takes a few seconds, largely reducing photodamage to living cells, resolving this issue effectively.

In this report, we used PbFRET to quantitatively assess the interaction of Bcl-XL and Bax in live HepG2 cells. Bcl-XL was expressed as fusion to the yellow fluorescent protein (YFP), and Bax was fused to the cyan fluorescent protein (CFP). We performed microscopic PbFRET imaging for living HepG2 cells co-expressing CFP-Bax and YFP-Bcl-XL on a wide-field fluorescence microscope, and found that Bcl-XL interacted directly with Bax, and their interaction on mitochondria was strong but modest in cytosol.

2. Materials and Methods

2.1. *Reagent and plasmids*

Turbofect™ *in vitro* transfection reagent was purchased from Fermentas Inc. (Glen Burnie, MD, USA). Cerulean, Venus-Kras and GFP-Bcl-2Cb5 plasmids were purchased from Addgene Company (Cambridge, MA). Plasmid of mCherry-Bad was kindly provided by Andrews.[6] Standard FRET constructs including C32V (Cerulean-32-Venus, Addgene plasmid 29396), CTV (C-TRAF-Venus, the TRAF is a tumor necrosis factor receptor-associated factor domain including 229 amino acid) and VCV (Venus-5-Cerulean-5-Venus, Addgene plasmid 27788) were kindly provided by the Vogel lab (National Institutes of Health, Bethesda, MD, USA). Plasmid DNA of CFP-Bax was kindly provided by Dr. Prehn.[20] Plasmid DNA of YFP-Bcl-XL was kindly provided by Prof. Youle.[13]

2.2. *Cell culture and transfection*

HepG2 cells, a human hepatocellular carcinoma cell line, were obtained from the Department of Medicine, Jinan University, Guangzhou, China. Cells were cultured in Dulbecco's modified Eagle's medium (DMEM, Gibco, Grand Island, New York) containing 10% fetal calf serum (FCS; Sijiqing, Hangzhou, China) at 37°C under 5% CO_2 in a humidified incubator. For transfection, cells were cultured in DMEM containing 10% FCS in a 35-mm glass dish with a density of 4×10^4 cells/ml at 37°C under 5% CO_2 in a humidified incubator. After 24 h, when the cells reached 70–90% confluence, plasmid was transfected into the HepG2 cells by using Turbofect™ *in vitro* transfection reagent in 35-mm dish for 24–48 h. Cells co-expressing CFP-Bax and YFP-Bcl-XL were treated with 5 μM Bcl-XL inhibitor ABT-737 (Merck-Calbiochem, USA) for 6 h or not.

2.3. *PbFRET imaging*

Partial acceptor photobleaching-based FRET imaging method (PbFRET), as a calibration-free method, was used to determine the FRET efficiency (E) of a FRET construct by measuring the degree of acceptor photobleaching (x) and the donor fluorescence intensity detected with donor channel that selectively collect donor fluorescence at donor excitation before (I_D) and after (I_{DP}) partial acceptor photobleaching. The E value of $1D{-}nA$ ("D" denotes donor molecule and "A" denotes acceptor molecule, n represents the number of acceptors in the FRET construct) construct is given as[28,30]

$$E = \frac{1 - I_D/I_{DP}}{1 - (1 - x/n)I_D/I_{DP}}, \tag{1}$$

where x is determined by monitoring the acceptor intensity with acceptor excitation before (I_A) and after (I_{AP}) photobleaching, which is given by $x = (I_A - I_{AP})/I_A$.

For PbFRET imaging, we first got the fluorescence images of donors with donor channel before (D) and after (DP) partially photobleaching acceptors and the fluorescence images of acceptors with acceptor channel before (A) and after (AP) partially photobleaching acceptors of FRET construct. To reduce errors due to cellular motility, we processed 3×3 bin smooth for the four fluorescence images. The autofluorescence of living HepG2 cells was found to be very low (data not shown). In the four fluorescence images, backgrounds were removed with average reading the same cell-devoid areas. We set an intensity value which was slightly greater than background as threshold intensity for each image. To improve image quality, we set the pixel intensity lower than the threshold intensity to be zero in each image. Then, we obtained the corresponding pixel-to-pixel E image and histogram of the living cells. Because of cellular motility and the randomness of protein expression level in living cells, the pixel-to-pixel E values had a distribution. To improve precision, we took the average of E values whose relative frequency was greater than one third in the corresponding E histogram as the E value of the image.

2.4. *Microscope platform*

Microscopic PbFRET imaging experiments were performed on a wide-field microscope (Axiovision, Carl Zeiss, Oberkochen, Germany) that was specifically designed for fast photobleaching to reduce errors caused by the cellular motility and fluorescence recovery as described previously.[31] This microscope is equipped with an X-cite 120Q Metal halide lamp, a 40×/NA 1.3 oil immersion objective, a CCD camera (C11440-22CU, HAMAMATSU PHOTONICS K.K., Hamamatsu, Japan) and 4-cube filters: D-cube, A-cube, GFP-cube and mCherry-cube. The filters and dichroic mirrors (Carl Zeiss, Oberkochen, Germany) in D (CFP/Cerulean)-cube, A (YFP/Venus)-cube, GFP-cube and mCherry-cube are BP 436/25 (436 nm excitation), BP 480/40 (emission), FT 455, BP 510/17 (510 nm excitation), LP 530 (emission), DFT 460 + 520, BP 500/20 (500 nm excitation), BP 535/30 (emission), DFT 515, and BP 565/30 (565 nm excitation), BP 620/60 (emission), FT 585, respectively. We introduced D-cube, A-cube, GFP-cube or mCherry-cube to the light-path of the wide-field microscope by filter wheels to selectively collect CFP/Cerulean, YFP/Venus, GFP or mCherry fluorescence. The excitation intensity is controlled by switching the different luminosity (0%, 12.5%, 25%, 50%, 100% of the total luminosity) of Metal halide lamp and/or turning the neutral density filters wheel between different attenuation degree (2%, 20%, 40%, 50%, 70%, 100%).

For PbFRET imaging of cells co-expressing CFP/Cerlean and YFP/Venus, 436 nm excitation was used to mainly excite CFP/Cerulean and 510 nm excitation was used to selectively excite YFP/Venus. The emission filter of D-cube, BP 480/40, was used to selectively detect the fluorescence of CFP/Cerulean, and the emission filter of A-cube, LP 530, was used to collect the YFP/Venus fluorescence.

For PbFRET imaging of cells co-expressing GFP and mCherry, 500 nm excitation was used to mainly excite GFP and 565 nm excitation was used to selectively excite mCherry. The emission filter of GFP-cube, BP 535/30, was used to selectively detect the fluorescence of GFP, and the emission filter of mCherry-cube, BP 620/60, was used to collect the mCherry fluorescence.

2.5. *Statistical analysis*

Results are expressed as mean ± SD. Data were analyzed by repeated-measures ANOVA with parametric methods using the statistical software

SPSS 18.0 (SPSS, Inc., Chicago, IL, USA). Throughout the work, P values less than 0.05 were considered to be statistically significant.

3. Results and Discussion

3.1. *Suitable excitation conditions*

Photobleaching of fluorophores during microscopic imaging should be rigorously controlled for quantitative FRET measurement. Therefore, it is necessary to select suitable excitation conditions to avoid photobleaching of both donor and acceptor fluorophores. Figure 1(a) shows the representative time-lapse images of living HepG2 cells separately expressing CFP-Bax residing evenly and YFP-Bcl-XL having clumped distribution. Figure 1(b) shows the corresponding dynamic fluorescence intensities of the two living cells in Fig. 1(a) during the time-lapse imaging with 0.5% transmission, the excitation transmission in our all experiments, of 436 nm or 510 nm excitation. The same results were also observed in ten cells separately expressing CFP-Bax and YFP-Bcl-XL. The constant fluorescence intensity indicated a negligible photobleaching for donor and acceptor fluorophores during imaging with 0.5% transmission.

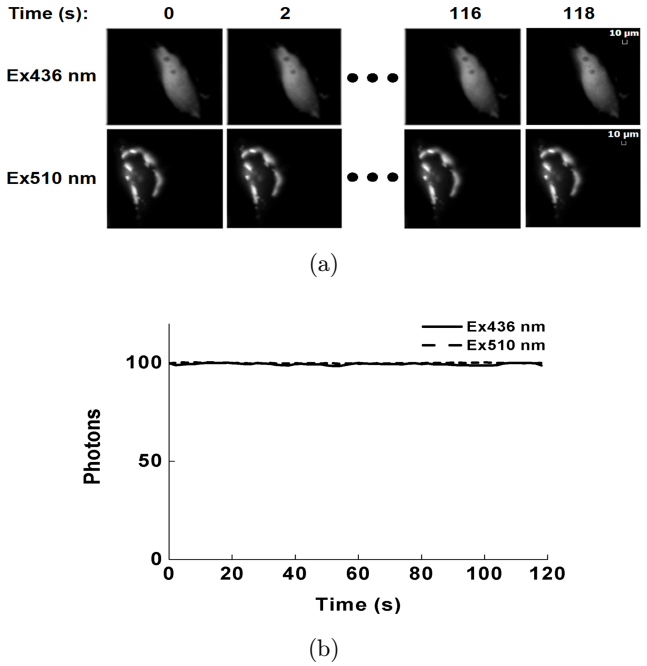

Fig. 1. Suitable excitation conditions for donor (CFP-Bax) and acceptor (YFP-Bcl-XL) in living cells. (a) Time-lapse images of living HepG2 cells separately expressing CFP-Bax with 436 nm excitation and YFP-Bcl-XL with 510 nm excitation. Scale bar: 10 μm. (b) Dynamics of fluorescence intensities of the two living cells in (a) during the time-lapse imaging.

High quality images could be obtained with 1% excitation transmission, but this strong illumination easily resulted in photobleaching (data not shown). It was obvious that YFP-Bcl-XL mainly distributed on mitochondria (Fig. 1(a)), similar to many other experimental results.[6,8] It was reported that about half of the Bcl-XL resided in the cytoplasm of living cells,[6] and the yellow fluorescence intensity in the cytoplasm was lower than that on mitochondria possibly due to the large cytoplasm areas. In reality, YFP-Bcl-XL fluorescence in the nonmitochondria area could be imaged clearly with stronger excitation which resulted in saturation and bleaching in mitochondria area (data not shown).

3.2. *Implementation of PbFRET for measuring the E value of C32V construct in living cells*

For PbFRET imaging, we used a 25% of 510 nm excitation to bleach partial acceptors. Figure 2(a) shows the representative fluorescence images of donors with D-cube before (D) and after (DP) partially photobleaching acceptors and that of acceptors with A-cube before (A) and after (AP) partially photobleaching acceptors of C32V. By using Eq. (1), we obtained the corresponding pixel-to-pixel pseudo-color E image (Fig. 2(b)) and histogram (Fig. 2(c)) of the living cells expressing C32V, and the corresponding E value was 27.99%. The average E of C32V measured by PbFRET method was $25.99 \pm 2.32\%$ ($n = 13$), consistent with the results of $28.67 \pm 0.95\%$ measured by modified spectral FRET quantification method (mlux-FRET).[32]

In the pseudo-color E image, we noted that the edges of some cells were crimson, which may be due to the low fluorescence intensity. PbFRET is not affected by imaging conditions and fluorophore properties such as quantum yields and extinction coefficients, so this method can be easily performed on most imaging systems without any additional references and system calibrations. However, there are three prerequisites for PbFRET implementation: (1) the photobleaching excitation must selectively photobleach acceptors; (2) the acceptor excitation selectively excites the acceptors to exclude the influence of donor fluorescence for the accurate determination of x; and (3) the donor

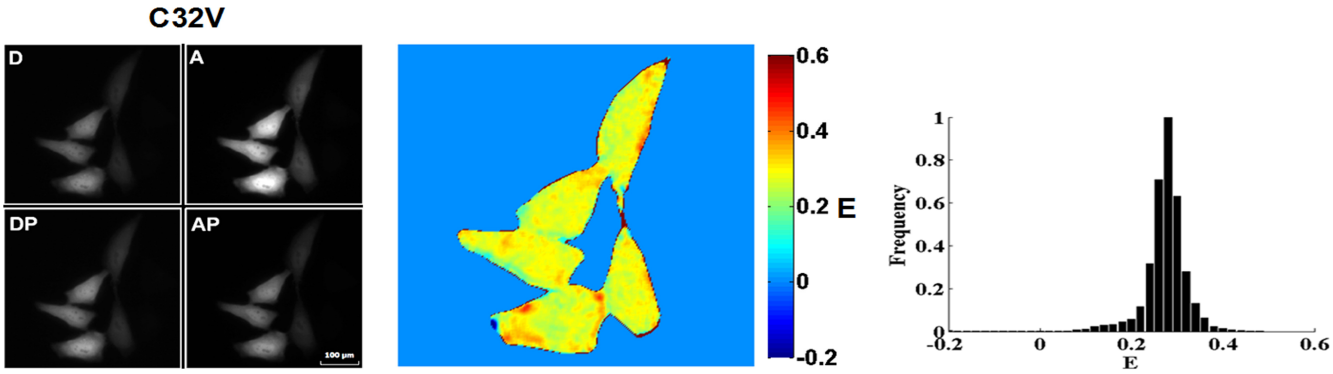

(a) (b) (c)

Fig. 2. Implementation of PbFRET for measuring the E value of C32V construct in living HepG2 cells. (a) Typical fluorescence images in both donor and acceptor channels before and after partially photobleaching acceptor. Scale bar: 100 μm. (b) Pixel-to-pixel FRET efficiency (E) image, and (c) the corresponding FRET efficiency (E) histogram of cells in (a).

detection channel is chosen to selectively detect the donor fluorescence.[31] It is generally difficult to choose an appropriate optical filter as a donor emission channel to selectively collect donor fluorescence for some FPs pairs with a large spectral overlap such as green fluorescent protein (GFP) and yellow fluorescent protein (YFP).[33] Furthermore, we should pay attention to turning the cube fast to reduce errors caused by the cellular motility and fluorescence recovery during the process of implementing PbFRET, and this imaging process can be accomplished at most 2 s on our platform.

3.3. *Validation of PbFRET imaging by measuring the E values of standard FRET constructs in living cells*

To validate PbFRET imaging, we implemented PbFRET imaging on our wide-field microscope for the living HepG2 cells expressing standard FRET constructs with different FRET efficiency. Figure 3(a) shows the representative fluorescence images of living HepG2 cells co-transfected with free Cerulean (C) and Venus-Kras (V). Figure 3(b) (upper) shows the image of a cell indicated by red square in Fig. 3(a) (left) and the fluorescence images of cells expressing CTV (middle) and VCV (right). The corresponding pixel-to-pixel pseudo-color E images and histograms were shown in Fig. 3(b) (middle and lower), and the corresponding E value was 0.93% for free C and V, 1.65% for CTV and 67.42% for VCV. The statistical E value from at least 30 live HepG2 cells in three independent experiments was 3.44 ± 5.34% for free C + V (Fig. 3(c)). The statistical E value from 12 frames was $2.82 \pm 2.60\%$ for CTV (Fig. 3(c)), consistent with the results of $6.3 \pm 2.6\%$ measured by fluorescence lifetime imaging microscopy (FLIM) and $1.7 \pm 7.0\%$ measured by spectral mixing-based method in Vogel's laboratory.[34] Cells expressing VCV from 15 frames had an average E value of $63.67 \pm 2.20\%$ (Fig. 3(c)), consistent with the value measured by our laboratory with Iem-spFRET method.[35]

For cells transfected with tandem constructs CTV or VCV, we directly measured the E value of the frame. However, for cells co-transfected with free C and V, there may be some cells only expressing C or V. Therefore, we selected the cells co-expressing C and V for PbFRET imaging (Fig. 3 (b)). We here substituted $n = 1$ into Eq. (1) to obtain E value of cells co-expressing C and V. In fact, for FRET construct with free donor and acceptor, the value of n was larger than 1 when acceptor concentration was higher than donor concentration. In this case, substituting n for 1 resulted in a decrease in the measured E value. We noted that the E value of the lower edge of the cell was low in the pseudo-color map of cell expressing C + V (Fig. 3(b), second row, first column), which may be due to lower level expression of C on the lower edge. We also noted that the E value of the upper edge of the cell was high in the pseudo-color map of cell expressing C + V (Fig. 3(b), second row, first column), which may be due to high level expression of both C and V on the upper edge. This inconsistent expression of donor and acceptor DNA fragments led to a wide E distribution for cell expressing

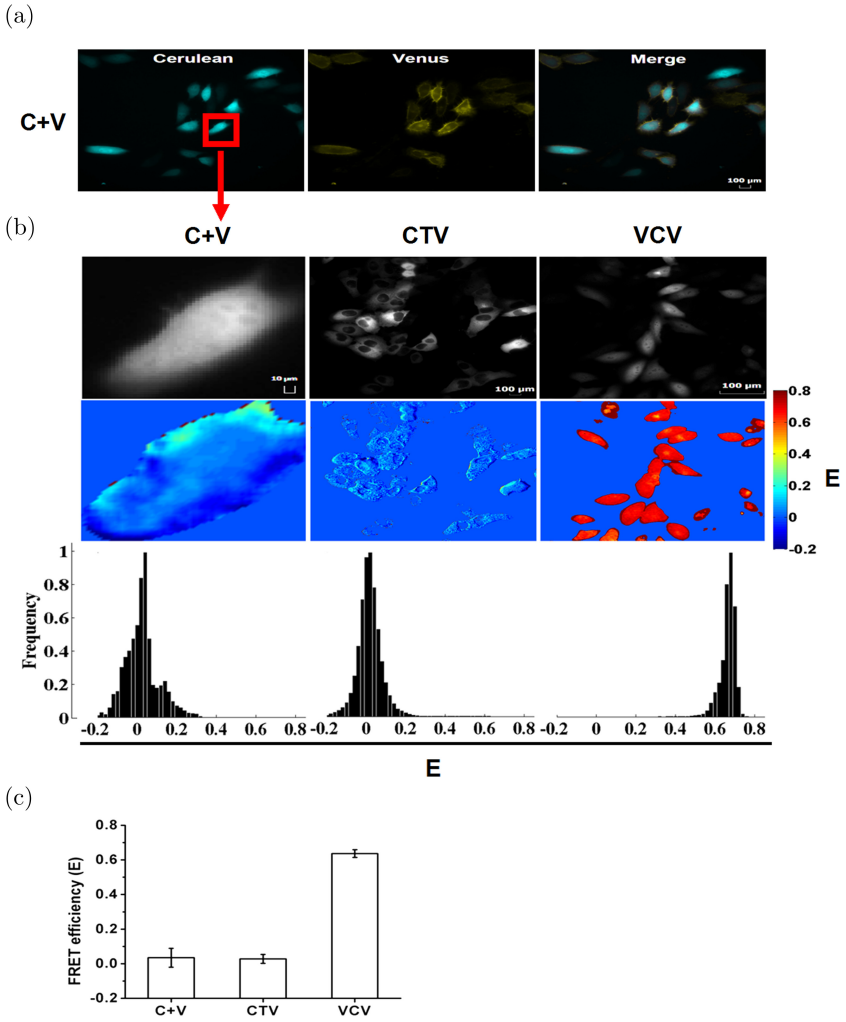

Fig. 3. Validation of PbFRET imaging by mapping the E values of standard FRET constructs in living HepG2 cells. (a) Representative fluorescence images of living HepG2 cells transfected with free Cerulean (C) and free Venus-Kras (V) in donor and acceptor channels. Cell in the red square co-expressing C and V. Scale bar: 100 μm. (b) Typical fluorescence images and the corresponding pixel-to-pixel E images as well as their histograms of cells expressing C + V, CTV and VCV, respectively. Scale bar: 10 μm or 100 μm. (c) Statistical E values of C + V, CTV and VCV constructs in living HepG2 cells.

C + V (Fig. 3(b), third row, first column). In addition, mobility of fluorescent molecules in living cells described in above paragraph may also result in the wide distribution of E values. Even so, it can be seen from our results that constructs with low or high FRET efficiency in living cells could be exactly quantified by PbFRET imaging method on our wide-field imaging system.

3.4. *Mapping Bax-Bcl-XL interaction in single living cells by PbFRET imaging*

We next used PbFRET imaging to map the interaction between CFP-Bax and YFP-Bcl-XL in single living HepG2 cells. Figure 4(a) (left) shows the representative fluorescence image of a living HepG2 cell co-expressing CFP-Bax and YFP-Bcl-XL, showing that CFP-Bax resided in cytoplasm uniformly and YFP-Bcl-XL had clumped distribution. Figures 4(b)–4(d) (left) show the corresponding pixel-to-pixel pseudo-color E images and histograms of nonmitochondria and mitochondria as well as whole cell area, and the corresponding E value was 4.41% for nonmitochondria area, and 12.57% for mitochondria area as well as 8.74% for the whole cell. The statistical E values from 27 living HepG2 cells were $4.59 \pm 2.66\%$ for nonmitochondria area, $11.31 \pm 5.47\%$ for mitochondria area and $7.16 \pm 2.91\%$ for the whole cell (Fig. 4(b)).

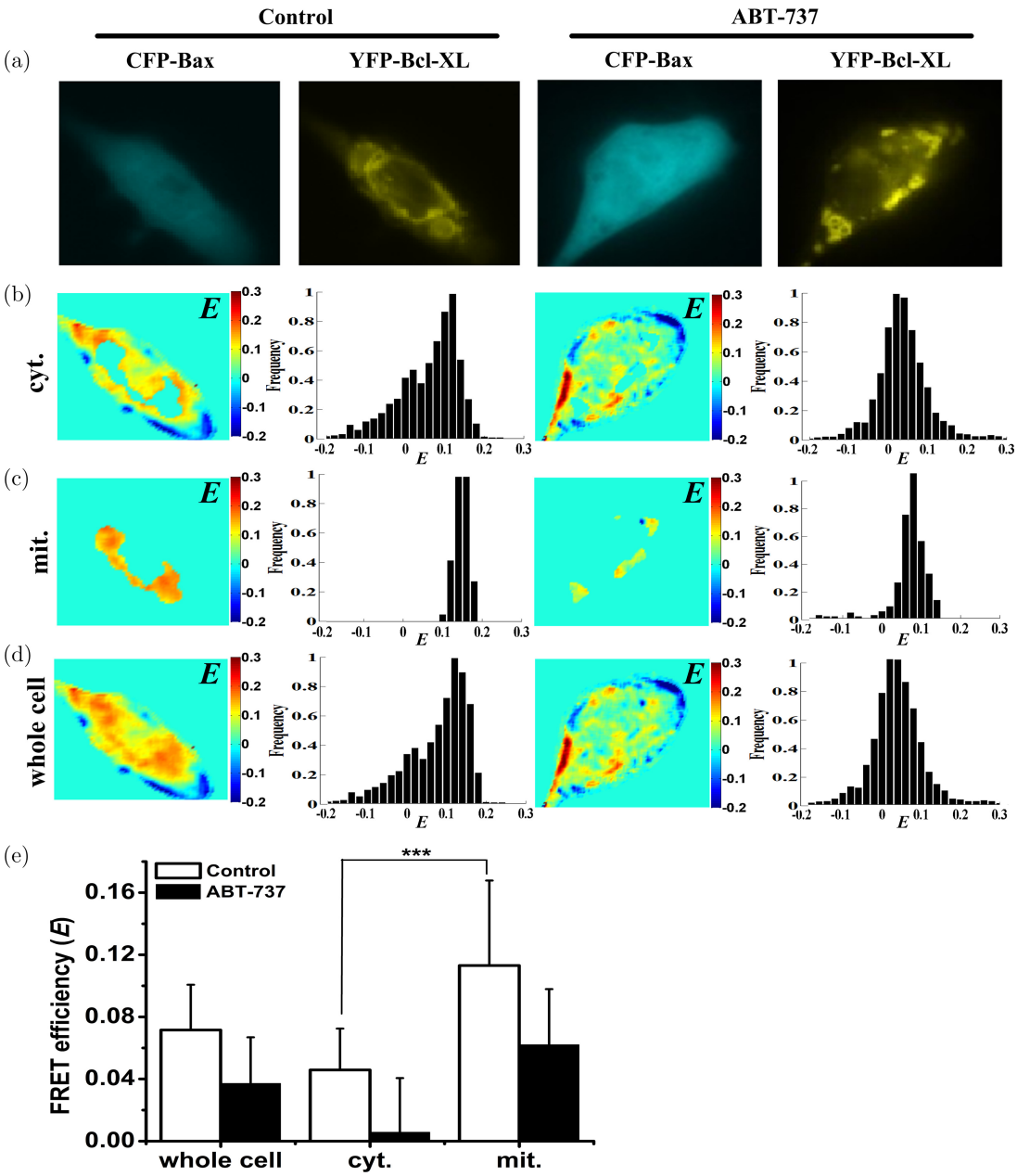

Fig. 4. Bax-Bcl-XL interaction in single living HepG2 cells by PbFRET imaging. (a) Representative fluorescence image of a living HepG2 cell co-expressing CFP-Bax and YFP-Bcl-XL with or without (control) ABT-737 treatment. Corresponding pixel-to-pixel pseudo-color E images and histograms of nonmitochondria area (cyt.) (b), mitochondria area (mit.) (c) as well as whole cell area (whole cell) (d) of the cells with or without ABT-737 treatment in (a). (e) Statistical E values of nonmitochondria area, mitochondria area and whole cell from 27 control cells and 17 ABT-737-treated cells. Data were analyzed by ANOVA; ns no significant, $^{*}p < 0.05$, $^{**}p < 0.01$, $^{***}p < 0.001$.

We chose the region where YFP-Bcl-XL had clumped distribution as mitochondria area, and we set an intensity value which was slightly greater than the intermediate intensity value of no-clumped area of YFP-Bcl-XL as threshold intensity to identify mitochondria for each cell, and the region where yellow fluorescence intensity was greater than the threshold intensity was considered as mitochondria area.

To further confirm the interaction between Bax and Bcl-XL, we examined the effect of the BH3 mimetic ABT-737,[6,36] an inhibitor of Bcl-XL, on the binding of Bax with Bcl-XL. We performed PbFRET analysis for living cells co-expressing

CFP-Bax and YFP-Bcl-XL in the presence of ABT-737, and Fig. 4(a) (right) shows the representative fluorescence image of a living HepG2 cell co-expressing CFP-Bax and YFP-Bcl-XL in the presence of ABT-737. Figures 4(b)–4(d) (right) show the corresponding pixel-to-pixel pesudo-color E images and histograms of nonmitochondria and mitochondria as well as whole cell area, and the corresponding E value was 3.57% for nonmitochondria area, and 7.75% for mitochondria area as well as 3.82% for the whole cell. The statistical E values from 17 living HepG2 cells in the presence of ABT-737 was $0.58 \pm 3.48\%$ for nonmitochondria area, $6.21 \pm 3.58\%$ for mitochondria and $3.71 \pm 2.97\%$ for the whole cell (Fig. 4(e)). The measured E values between CFP-Bax and YFP-Bcl-XL in the presence of ABT-737 were always significantly lower than those in the absence of ABT-737 (Fig. 4(e)), confirming the interaction between Bax and Bcl-XL, and suggesting that ABT-737 inhibited the interaction between Bax and Bcl-XL.

PbFRET imaging can track protein–protein interaction not only in mitochondria but also in other organelles (such as endoplasmic reticulum (ER)). We performed PbFRET assay for the ER regions of living cells co-expressing GFP-Bcl-2Cb5 (the ER-targeted GFP-Bcl-2, the ER-targeting domain of cytochrome b_5 (amino acids 100-134) was used to replace amino acids 217-239 of Bcl-2)[37] and mCherry-Bad (Fig. 5). The statistical E values between GFP-Bcl-2Cb5 and mCherry-Bad from about 30 living cells was $8.04 \pm 7.21\%$ in ER and $11.23 \pm 7.68\%$ in non-ER area (Fig. 5(d)), indicating that Bcl-2 interacted directly with Bad in ER and non-ER area. We chose the region where GFP-Bcl-2Cb5 has clumped distribution as ER area, and we set an intensity value which was slightly greater than the intermediate intensity value of no-clumped area of GFP-Bcl-2Cb5 as threshold intensity to identify ER for each cell, and the region where green fluorescence intensity was greater than the threshold intensity was considered as ER area.

Many *in vitro* studies on the Bax-Bcl-XL interaction have been carried out.[12,14,18] FRAP and FLIP were recently used to indirectly examine their interaction in living cells, and suggested that Bcl-XL retrotranslocates Bax from the mitochondria into the cytosol after their transient interaction on mitochondria.[3] According to this view, Bax and Bcl-XL has a strong interaction on mitochondria but a weak interaction in nonmitochondria area, which is consistent with our FRET data that CFP-Bax and YFP-Bcl-XL has a high E value (11.31%) on mitochondria and a lower E value (4.59%) in nonmitochondria area. Considering the 3.44% of E value for cells coexpressing free C and V, the 4.59% of E value between CFP-Bax + YFP-Bcl-XL in nonmitochondria area was very modest, indicating the very weak interaction between Bax and Bcl-XL proteins in nonmitochondria area. In reality, the mitochondria out of the focal plane might be regarded as nonmitochondria area, which may result in an increase in the measured E value between CFP-Bax and YFP-Bcl-XL in nonmitochondria area. However, the E value obtained by PbFRET method is the apparent FRET efficiency normalized to donor concentration.[28] Moreover, the lower E value between CFP-Bax and YFP-Bcl-XL in nonmitochondria area may be ascribed to the higher concentration of CFP-Bax than YFP-Bcl-XL just described above. In the presence of free donor and/or acceptor, it is important to simultaneously ascertain FRET efficiency and the total concentration ratio of acceptor to donor for the accurate interpretation of FRET signal. However, PbFRET method can't ascertain the concentration ratio of acceptor to donor. Therefore, we will use sensitized emission-based[38,39] or spectral unmixing-based[35] FRET quantification method to study the interaction of Bax and Bcl-XL in live cells in the near future.

11.31% of E value between CFP-Bax + YFP-Bcl-XL in mitochondria area was significantly greater than that in nonmitochondria area (Fig. 4(e)), showing that Bax and Bcl-XL had strong interaction in mitochondria area or Bcl-XL bound Bax tightly on mitochondria before it retrotranslocated Bax back into the cytoplasm. We here took 1 as the value of n for cell co-expressing CFP-Bax and YFP-Bcl-XL. In fact, YFP-Bcl-XL concentration was greater than CFP-Bax concentration on mitochondria. Therefore, lower value of n may result in a decrease in the measured E value between CFP-Bax and YFP-Bcl-XL in mitochondria area. These results support the notion that Bcl-XL inhibits and maintains Bax in the cytosol by constant retrotranslocation of mitochondrial Bax.[3] In reality, it was inaccurate by comparing yellow fluorescence intensity with the threshold intensity to distinguish mitochondria and nonmitochondria area. Therefore, we will use MitoTracker Deep Red (MTDR) to probe mitochondria in the near future.

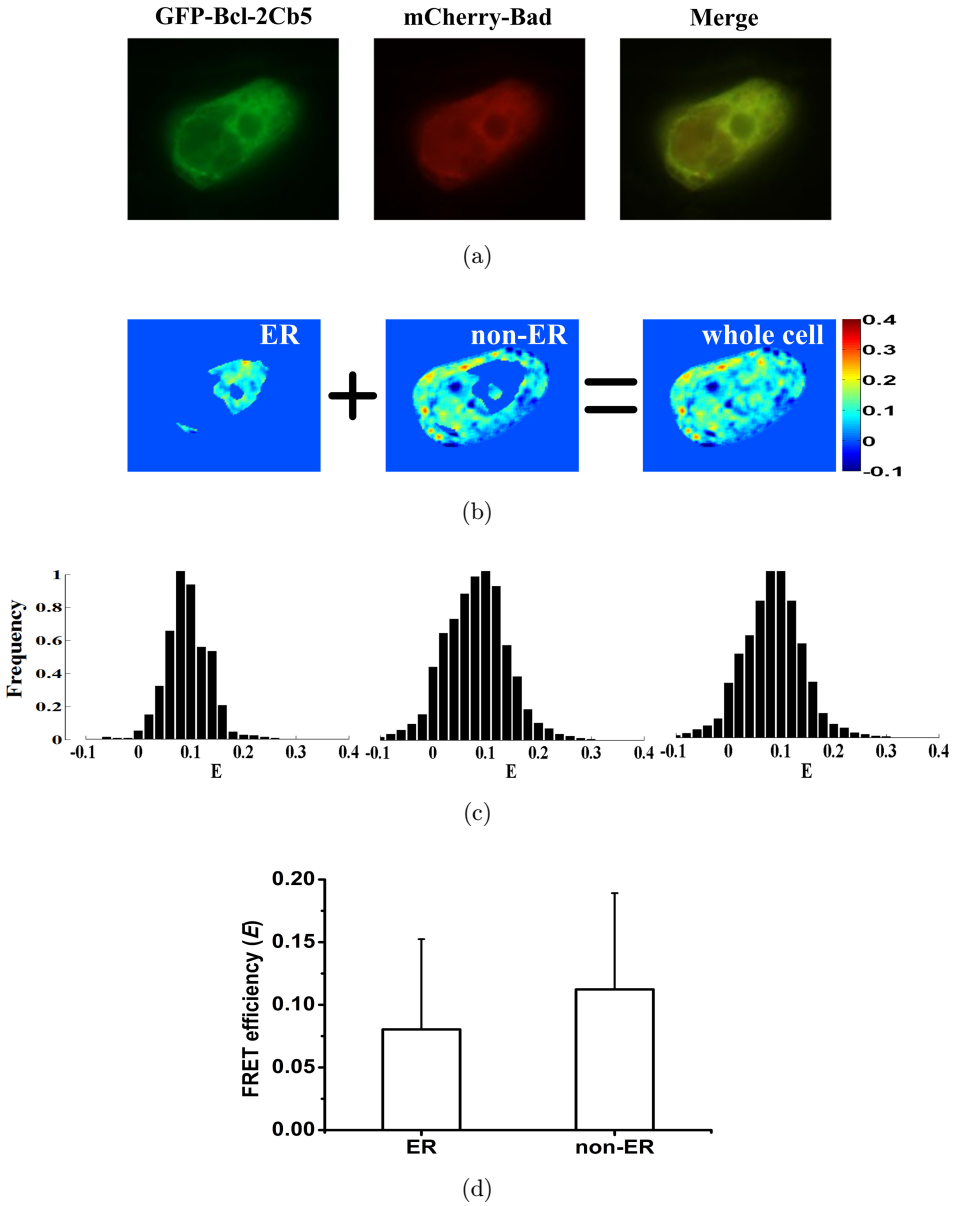

Fig. 5. Bcl-2-Bad interaction in endoplasmic reticulum (ER) by PbFRET imaging. (a) Representative fluorescence images of a living HepG2 cell co-expressing GFP-Bcl-2Cb5 and mCherry-Bad. Corresponding pixel-to-pixel pseudo-color E images (b) and histograms (c) of ER area (ER), non-ER area (non-ER) as well as whole cell area (whole cell) of the cell in (a). (d) Statistical E values of ER area and non-ER area from about 30 living cells.

4. Conclusion

PbFRET imaging is applicable to mapping protein-protein interactions in single live cells. Bcl-XL interacts directly with Bax in healthy HepG2 cells, and especially their interaction is strong on mitochondria but modest in cytosol, which supports the notion that Bcl-XL on mitochondria inhibits Bax oligomerization and activation by directly interacting with Bax and subsequently retrotranslocating Bax from mitochondria back into cytosol.

Acknowledgments

The authors thank Prof. S. S. Vogel (NIH/NIAAA) for providing C32V, CTV and VCV plasmids, Prof. J. Prehn for providing CFP-Bax plasmid and Prof. R. J. Youle for providing YFP-Bcl-XL plasmid.

This work was supported by the National Natural Science Foundation of China (NSFC) (Grant Nos. 61527825, 61875056 and 81572184).

References

1. J. M. Adams, S. Cory, "The Bcl-2 apoptotic switch in cancer development and therapy," *Oncogene* **26** (9), 1324–1337 (2007).
2. J. K. Brunelle, A. Letai, "Control of mitochondrial apoptosis by the Bcl-2 family," *J. Cell Sci.* **122**(4), 437–441 (2009).
3. F. Edlich, S. Banerjee, M. Suzuki, M. M. Cleland, D. Arnoult, C. Wang, A. Neutzner, N. Tjandra, R. J. Youle, "Bcl-x(L) retrotranslocates Bax from the mitochondria into the cytosol," *Cell* **145**(1), 104–116 (2011).
4. M. C. Wei, W. X. Zong, E. H. Y. Cheng, T. Lindsten, V. Panoutsakopoulou, A. J. Ross, K. A. Roth, G. R. MacGregor, C. B. Thompson, S. J. Korsmeyer, "Proapoptotic BAX and BAK: A requisite gateway to mitochondrial dysfunction and death," *Science* **292**(5517), 727–730 (2001).
5. K. G. Wolter, Y. T. Hsu, C. L. Smith, A. Nechushtan, X. G. Xi, R. J. Youle, "Movement of Bax from the cytosol to mitochondria during apoptosis," *J. Cell Biol.* **139**(5), 1281–1292 (1997).
6. A. Aranovich, Q. Liu, T. Collins, F. Geng, S. Dixit, B. Leber, D. W. Andrews, "Differences in the mechanisms of proapoptotic BH3 proteins binding to Bcl-XL and Bcl-2 quantified in live MCF-7 cells," *Mol. Cell* **45**(6), 754–763 (2012).
7. G. Hausmann, L. A. O'Reilly, R. van Driel, J. C. Beaumont, A. Strasser, J. M. Adams, D. C. Huang, "Pro-apoptotic apoptosis protease-activating factor 1 (Apaf-1) has a cytoplasmic localization distinct from Bcl-2 or Bcl-x(L)," *J. Cell Biol.* **149**(3), 623–634 (2000).
8. Y. T. Hsu, K. G. Wolter, R. J. Youle, "Cytosol-to-membrane redistribution of Bax and Bcl-XL during apoptosis," *Proc. Natl. Acad. Sci. USA* **94** (8), 3668–3672 (1997).
9. D. Nijhawan, M. Fang, E. Traer, Q. Zhong, W. Gao, F. Du, X. Wang, "Elimination of Mcl-1 is required for the initiation of apoptosis following ultraviolet irradiation," *Genes Dev.* **17**(12), 1475–1486 (2003).
10. T. W. Sedlak, Z. N. Oltvai, E. Yang, K. Wang, L. H. Boise, C. B. Thompson, S. J. Korsmeyer, "Multiple Bcl-2 family members demonstrate selective dimerizations with Bax," *Proc. Natl. Acad. Sci. USA* **92** (17), 7834–7838 (1995).
11. E. Yang, J. Zha, J. Jockel, L. H. Boise, C. B. Thompson, S. J. Korsmeyer, "Bad, a heterodimeric partner for Bcl-XL and Bcl-2, displaces Bax and promotes cell death," *Cell* **80**(2), 285–291 (1995).
12. Y. T. Hsu, R. J. Youle, "Nonionic detergents induce dimerization among members of the Bcl-2 family," *J. Biol. Chem.* **272**(21), 13829–13834 (1997).
13. S. Y. Jeong, B. Gaume, Y. J. Lee, Y. T. Hsu, S. W. Ryu, S. H. Yoon, R. J. Youle, "Bcl-x(L) sequesters its C-terminal membrane anchor in soluble, cytosolic homodimers," *EMBO J.* **23**(10), 2146–2155 (2004).
14. L. P. Billen, C. L. Kokoski, J. F. Lovell, B. Leber, D. W. Andrews, "Bcl-XL inhibits membrane permeabilization by competing with Bax," *PLoS Biol.* **6**(6), e147 (2008).
15. T. T. Renault, O. Teijido, B. Antonsson, L. M. Dejean, S. Manon, "Regulation of Bax mitochondrial localization by Bcl-2 and Bcl-xL: Keep your friends close but your enemies closer," *Int. J. Biochem. Cell Biol.* **45**(1), 64–67 (2013).
16. F. Llambi, T. Moldoveanu, S. W. Tait, L. Bouchier-Hayes, J. Temirov, L. L. McCormick, C. P. Dillon, D. R. Green, "A unified model of mammalian BCL-2 protein family interactions at the mitochondria," *Mol. Cell* **44**(4), 517–531 (2011).
17. B. Schellenberg, P. Wang, J. A. Keeble, R. Rodriguez-Enriquez, S. Walker, T. W. Owens, F. Foster, J. Tanianis-Hughes, K. Brennan, C. H. Streuli, A. P. Gilmore, "Bax exists in a dynamic equilibrium between the cytosol and mitochondria to control apoptotic priming," *Mol. Cell* **49**(5), 959–971 (2013).
18. T. T. Renault, O. Teijido, F. Missire, Y. T. Ganesan, G. Velours, H. Arokium, F. Beaumatin, R. Llanos, A. Athane, N. Camougrand, M. Priault, B. Antonsson, L. M. Dejean, S. Manon, "Bcl-xL stimulates Bax relocation to mitochondria and primes cells to ABT-737," *Int. J. Biochem. Cell Biol.* **64**, 136–146 (2015).
19. F. Todt, Z. Cakir, F. Reichenbach, R. J. Youle, F. Edlich, "The C-terminal helix of Bcl-x(L) mediates Bax retrotranslocation from the mitochondria," *Cell Death Differ.* **20**(2), 333–342 (2013).
20. H. Dussmann, M. Rehm, C. G. Concannon, S. Anguissola, M. Wurstle, S. Kacmar, P. Voller, H. J. Huber, J. H. Prehn, "Single-cell quantification of Bax activation and mathematical modelling suggest pore formation on minimal mitochondrial Bax accumulation," *Cell Death Differ.* **17**(2), 278–290 (2010).
21. R. Heim, R. Y. Tsien, "Engineering green fluorescent protein for improved brightness, longer wavelengths and fluorescence resonance energy transfer," *Curr. Biol.* **6**(2), 178–182 (1996).
22. E. A. Jares-Erijman, T. M. Jovin, "Imaging molecular interactions in living cells by FRET

microscopy," *Curr. Opin. Chem. Biol.* **10**(5), 409–416 (2006).

23. M. Mohsin, M. Z. Abdin, L. Nischal, H. Kardam, A. Ahmad, "Genetically encoded FRET-based nanosensor for in vivo measurement of leucine," *Biosens. Bioelectron.* **50**, 72–77 (2013).
24. A. K. Kenworthy, M. Edidin, "Distribution of a glycosylphosphatidylinositol-anchored protein at the apical surface of MDCK cells examined at a resolution of <100 Å using imaging fluorescence resonance energy transfer," *J. Cell Biol.* **142**(1), 69–84 (1998).
25. F. S. Wouters, P. I. Bastiaens, K. W. Wirtz, T. M. Jovin, "FRET microscopy demonstrates molecular association of non-specific lipid transfer protein (nsL-TP) with fatty acid oxidation enzymes in peroxisomes," *EMBO J.* **17**(24), 7179–7189 (1998).
26. H. Yu, J. Zhang, H. Li, T. Chen, "Ma-PbFRET: Multiple acceptors FRET measurement based on partial acceptor photobleaching," *Microsc. Microanal.* **19**(1), 171–179 (2013).
27. S. Lalonde, D. W. Ehrhardt, D. Loque, J. Chen, S. Y. Rhee, W. B. Frommer, "Molecular and cellular approaches for the detection of protein-protein interactions: Latest techniques and current limitations," *Plant J.* **53**(4), 610–635 (2008).
28. A. D. Elder, A. Domin, G. K. Schierle, C. Lindon, J. Pines, A. Esposito, C. F. Kaminski, "A quantitative protocol for dynamic measurements of protein interactions by Forster resonance energy transfer-sensitized fluorescence emission," *J. R. Soc. Interface* **6**(S1), S59–S81 (2009).
29. L. Wang, T. Chen, J. Qu, X. Wei, "Photobleaching-based quantitative analysis of fluorescence resonance energy transfer inside single living cell," *J. Fluoresc.* **20**(1), 27–35 (2010).
30. H. Yu, J. Zhang, H. Li, J. Qu, T. Chen, "An empirical quantitative fluorescence resonance energy transfer method for multiple acceptors based on partial acceptor photobleaching," *Appl. Phys. Lett.* **100**(25), 253701 (2012).
31. L. Zhang, H. Yu, J. Zhang, T. Chen, "Binomial distribution-based quantitative measurement of multiple-acceptors fluorescence resonance energy transfer by partially photobleaching acceptor," *Appl. Phys. Lett.* **104**(24), 243706 (2014).
32. L. Chai, J. Zhang, L. Zhang, T. Chen, "Miniature fiber optic spectrometer-based quantitative fluorescence resonance energy transfer measurement in single living cells," *J. Biomed. Opt.* **20**(3), 037008 (2015).
33. T. Zimmermann, J. Rietdorf, A. Girod, V. Georget, R. Pepperkok, "Spectral imaging and linear unmixing enables improved FRET efficiency with a novel GFP2-YFP FRET pair," *FEBS Lett.* **531**(2), 245–249 (2002).
34. C. Thaler, S. V. Koushik, P. S. Blank, S. S. Vogel, "Quantitative multiphoton spectral imaging and its use for measuring resonance energy transfer," *Biophys. J.* **89**(4), 2736–2749 (2005).
35. J. Zhang, H. Li, L. Chai, L. Zhang, J. Qu, T. Chen, "Quantitative FRET measurement using emission-spectral unmixing with independent excitation crosstalk correction," *J. Microsc.* **257**(2), 104–116 (2015).
36. M. Bruncko, T. K. Oost, B. A. Belli, H. Ding, M. K. Joseph, A. Kunzer, D. Martineau, W. J. McClellan, M. Mitten, S. C. Ng, P. M. Nimmer, T. Oltersdorf, C. M. Park, A. M. Petros, A. R. Shoemaker, X. Song, X. Wang, M. D. Wendt, H. Zhang, S. W. Fesik, S. H. Rosenberg, S. W. Elmore, "Studies leading to potent, dual inhibitors of Bcl-2 and Bcl-xL," *J. Med. Chem.* **50**(4), 641–662 (2007).
37. N. S. Wang, M. T. Unkila, E. Z. Reineks, C. W. Distelhorst, "Transient expression of wild-type or mitochondrially targeted Bcl-2 induces apoptosis, whereas transient expression of endoplasmic reticulum-targeted Bcl-2 is protective against Bax-induced cell death," *J. Biol. Chem.* **276**(47), 44117–44128 (2001).
38. T. Zal, N. R. Gascoigne, "Photobleaching-corrected FRET efficiency imaging of live cells," *Biophys. J.* **86**(6), 3923–3939 (2004).
39. H. Chen, H. L. Puhl, S. V. Koushik, S. S. Vogel, S. R. Ikeda, "Measurement of FRET efficiency and ratio of donor to acceptor concentration in living cells," *Biophys. J.* **91**(5), L39–L41 (2006).